Journal of Applied Physics

RESEARCH ARTICLE | JANUARY 11 2023

Mechanism of enhanced critical fields and critical current densities of MgB_2 wires with C/Dy_2O_3 co-additions

F. Wan ; M. D. Sumption ; E. W. Collings

J. Appl. Phys. 133, 023905 (2023)
https://doi.org/10.1063/5.0130589

Journal of Applied Physics ARTICLE scitation.org/journal/jap

Mechanism of enhanced critical fields and critical current densities of MgB_2 wires with C/Dy_2O_3 co-additions

Cite as: J. Appl. Phys. **133**, 023905 (2023); doi: 10.1063/5.0130589
Submitted: 12 October 2022 · Accepted: 21 December 2022 ·
Published Online: 11 January 2023

F. Wan,[1,2,a)] M. D. Sumption,[1] and E. W. Collings[1]

AFFILIATIONS

[1]Center for Superconducting and Magnetic Materials, Department of Materials Science and Engineering, The Ohio State University, Columbus, Ohio 43210, USA
[2]Fermi National Accelerator Laboratory, Batavia, Illinois 60510, USA

[a)]**Author to whom correspondence should be addressed:** fangwan@fnal.gov

ABSTRACT

A series of monofilamentary powder-in-tube MgB_2 wires were fabricated with 2 mol. % C doping and co-additions of 0–3 wt. % Dy_2O_3. Irreversibility fields ($\mu_0 H_{irr}$), upper critical fields ($\mu_0 H_{c2}$), and transport critical currents were measured, and from these quantities, anisotropies (γ) and electronic diffusivities ($D_{\pi,\sigma}$) were estimated. The addition of 1 wt. % Dy_2O_3 to already optimally C-doped MgB_2 wires produced higher $H_{c2//ab}$, $H_{c2//c}$, and H_{irr} values at 4.2 K. In addition, the critical current density, J_c, increased with Dy_2O_3 concentration up to 1 wt. % where non-barrier J_c reached 4.35×10^4 A/cm^2 at 4.2 K, 10 T. At higher temperatures, for example, 20 K and 5 T, co-additions of 2 mol. % C and 2 wt. % Dy_2O_3 improved non-barrier J_c by 40% and 93% compared to 2 and 3 mol. % C doping, respectively. On the other hand, measurements of T_c showed that C/Dy_2O_3 co-additions increase interband scattering rates at a lower rate than C doping does (assuming C doping levels giving similar levels of low-T $\mu_0 H_{c2}$ increase as co-addition). Comparisons to a two-band model for $\mu_0 H_{c2}$ in MgB_2 allowed us to conclude that the increases in $H_{c2//ab}$, $H_{c2//c}$, and H_{irr} (as well as concomitant increases in high-field J_c) with Dy_2O_3 addition are consistent with increases primarily in intraband scattering. This suggests C/Dy_2O_3 co-addition to be a more promising candidate for improving non-barrier J_c of MgB_2 at temperatures above 20 K.

I. INTRODUCTION

Investigation into the in-field performance of MgB_2 is complicated by its multi-band (gap) structure.[1] Two σ bands are derived from the in-plane, sp2 hybridized orbitals of B; these σ bands are two-dimensionally distributed within the B layers. In addition, two π bands are derived from the π-bonding and antibonding of the out-of-plane p_z orbitals; these π bands are three-dimensionally distributed throughout the lattice.[2,3] For an MgB_2 single crystal, this multi-band mechanism results in two upper critical fields $\mu_0 H_{c2//c}$ and $\mu_0 H_{c2//ab}$ and a resultant anisotropy $\gamma = H_{c2//ab}/H_{c2//c}$, where *//c* and *//ab* indicate two magnetic field directions—parallel to the *c*-axis and the *ab*-plane, respectively.[4] Of course, the superconducting properties of an MgB_2 polycrystalline sample or a wire are also affected by the multi-band mechanism, although the manifestation is slightly different. For a polycrystalline wire, e.g., $\mu_0 H_{c2}$ and $\mu_0 H_{irr}$ can be extracted from a ρ vs $\mu_0 H$ (ρ vs T) curve, taking $\mu_0 H_{c2}$ as $0.9\rho_n$ and $\mu_0 H_{irr}$ as $0.1\rho_n$, where ρ_n is the normal state resistivity. If each grain in a polycrystalline MgB_2 sample is assumed to be a single-crystal superconducting domain having constant $H_{c2//c}$ and $H_{c2//ab}$, the H_{c2} of the polycrystalline MgB_2 will be equivalent to $H_{c2//ab}$, indicating the critical field where the last (first) MgB_2 grain exhibits superconducting-normal state transition in increasing (decreasing) magnetic field. Thus, in this work, H_{c2} always corresponds to $H_{c2//ab}$ unless otherwise noted. On the other hand, H_{irr} is tied to $H_{c2//c}$.

One of the main reasons to pursue higher critical fields is for the superconductor in question to be able to exhibit supercurrents in higher magnetic fields. However, in addition to higher critical fields, sufficient flux pinning and MgB_2 connectivity are required. In terms of direct attempts to increase connectivity, a number of mechanical pressing methods have been applied to PIT *in-situ*

MgB_2 wires in order to improve their grain connectivity. Two typical mechanical pressing methods investigated have been hot isostatic pressing (HIP)[5,6] and cold-high-pressure-densification (CHPD).[7–9] Gajda *et al.* showed that HIP induced the formation of high-density and high-uniformity MgB_2 and increased J_cs three times at both 4.2 and 20 K.[5] Hossain *et al.* showed that transport J_cs and H_{irr}s of 10 wt. % $C_4H_6O_5$-added MgB_2 conductors cold-densified at 1.48 GPa were significantly enhanced at 20 K.[7]

On the other hand, dozens of dopants and additives have been investigated. Carbon doping is the most commonly used method to improve the high field transport J_cs of MgB_2 conductors, which it does mainly through increasing its upper critical fields. Carbon can be added in many forms, including SiC,[10–15] nanocarbon,[16–18] C_{60},[19] carbohydrate,[20,21] as well as by the use of C-predoped amorphous B powder.[22,23] Significant J_c improvement at high temperature was achieved by adding rare earth (RE) oxides into undoped MgB_2 or C-doped MgB_2.[24–29] It has been seen that adding RE oxides into MgB_2 can significantly increase flux pinning and therefore increase $J_c(\mu_0 H)$ due to the formation of REB_y (y = 4 or 6) and MgO nanoinclusions within the MgB_2 matrix. For example, Chen *et al.* reported that in-field J_cs were increased while lattice parameters and T_cs were unchanged for MgB_2 bulks pinned with DyB_4 inclusions for 0.5–5.0 wt. % additions of Dy_2O_3.[27] This is because these nano-inclusions can act both directly as flux pinning centers as well as acting to increase the density of grain boundaries.[27,30] However, Dy_2O_3 also has been seen to increase H_{irr}, indicating that Dy_2O_3 addition also decrease the electronic diffusivities, since H_{irr} is tied to $H_{c2//c}$. Yang *et al.* showed nano-sized Dy-based precipitates distributed in the grains of MgB_2 conductors doped with 0.5 wt. % Dy_2O_3 did not alter T_cs, but led to uniform 1T increase in H_{irr} over a wide range of temperatures.[31] These studies point out clearly that Dy_2O_3 reacts during heat treatment to form intragrain and intergrain nanoscale DyB_4 precipitates but does not substitute into MgB_2 lattice; therefore, the increased H_{irr} seems to be not related to the atomic substitution into the Mg or B sublattice. To date, however, there is not complete set of magnetic and transport data taken on the same series of MgB_2 strands with various Dy_2O_3 compositions, and hence, the effects of Dy_2O_3 addition on transport $J_c(\mu_0 H)$, $H_{irr}(T)$, and $H_{c2}(T)$ behavior of MgB_2 have not yet been fully explored.

In this work, a systematic study was conducted on J_cs and critical fields ($H_{c2//ab}$, $H_{c2//c}$, and H_{irr}) for a series of Dy_2O_3/C co-added powder-in-tube *in situ* MgB_2 wires, which were then compared to the results for a C-doped-only wire. The first aim is to fully investigate the temperature dependence of H_{irr} and H_{c2} for Dy_2O_3/C co-added MgB_2 wires over a wide temperature range (4.2–30 K). In addition, C/Dy_2O_3 co-addition is compared with C doping, and it is shown that the co-addition can improve MgB_2 performance over a wide temperature range. The results, with the aid of a two-band model for H_{c2} in MgB_2, are interpreted in terms of intra- and inter-band scattering with C/Dy_2O_3 co-additions.

II. EXPERIMENTAL DETAILS

A series of monofilamentary MgB_2 wires with C and Dy_2O_3 additions were fabricated by Hyper Tech Research Inc. (HTR). The wires were fabricated using mixed powders of Mg (<40 μm, 99%), "2 mol. % C-pre-doped" B (10–100 nm in size provided by Specialty Materials Inc. SMI), and Dy_2O_3 (99.9%, 100 nm, Sigma Aldrich) filled into a Nb tube surrounded by a Monel tube. After full reaction between Mg, pre-doped B, and Dy_2O_3, the wires have actual C-doping level of 2.10 mol. %[32] and Dy_2O_3 concentrations of 0.0, 1.0, 2.0, and 3.0 wt. % with respect to MgB_2. The wires have a 0.84 mm outer diameter and were heat-treated (HT) either at 650 °C/1h or at 675 °C/2h and were then furnace cooled to room temperature.

Resistivity, $R(T)$, was measured from 15 to 45 K in transverse magnetic fields ranging from 0.005 to 12 T. These $R(T)$ measurements were conducted on 10 mm segments of the 0.0 and 1.0 wt. % Dy_2O_3-added samples using a Quantum Design Model 6000 Physical Property Measuring System (PPMS) as described in Ref. 33. Values of $\mu_0 H_{c2}$ and $\mu_0 H_{irr}$ were extracted from $R(T)$ curves at $0.9R_n$ and $0.1R_n$, respectively. $\mu_0 H_{c2}$ and $\mu_0 H_{irr}$ data at 4.2 K for 0.0 and 1.0 wt. % Dy_2O_3-added samples were obtained from measurements of resistivity as a function of magnetic field, $R(\mu_0 H)$, measured in liquid helium in fields up to 30 T in a resistive magnet at the National High Magnetic Field Laboratory. Transport 4.2 K I_c measurements were performed at OSU at pool boiling liquid helium as a function of transverse magnetic field, H, up to 12.5 T on 5 cm-long-segments of selected wires using a four-point-probe method. Transport I_cs were extracted from the V–I curves using a gauge length of 5 mm and an electric field criterion of 1.0 μV cm^{-1}. Non-barrier J_cs of these PIT MgB_2 wires were calculated by dividing the conductor I_c value by the MgB_2 filamentary area (summed over the whole strand), and this is the same as the area inside the Nb chemical barrier.

III. RESULTS

A. Critical current densities

Figure 1 shows the 4.2 K transport non-barrier J_cs as a function of transverse magnetic field for samples with 2 mol. % C doping and Dy_2O_3 compositions from 0 to 3 wt. % (all additions in this work are with respect to the final MgB_2). The non-barrier J_cs of 2 mol. % C-doped-only samples (Dy0.0-C2-650 and Dy0.0-C2-675) reported in Refs. 34 and 35 are included in Figs. 1(a) and 1(b), respectively, for comparison. Also shown in Figs. 1(a) and 1(b) are non-barrier J_cs of a 2 mol. % C/0.5 wt. % Dy_2O_3 co-added MgB_2 wire HT at 675 °C (Dy0.5-C2-675).[31] At both HT conditions, the 1.0 wt. % Dy_2O_3 addition (with baseline 2 mol. % C doping) achieved the highest transport J_cs (e.g., 3.08×10^4 A/cm^2 for Dy1.0-C2-650 and 4.35×10^4 A/cm^2 for Dy1.0-C2-675 at 4.2 K, 10 T). Increasing Dy_2O_3 concentration from 1.0 wt. % to higher values (2.0 and 3.0 wt. %) reduced J_c slightly from this maximum value to 3.28×10^4 and 2.96×10^4 A/cm^2, respectively. We will argue below that the main contribution to this behavior has to do with H_{c2} increases associated with additional intraband scattering with increasing Dy_2O_3 additions, although there may also be a contribution-enhanced pinning associated with DyB_4 and MgO nanoinclusions[36,37] that have collected at the grain boundaries.

From Figs. 1(a) and 1(b), it can be seen that the most important difference with 1.0 wt. % Dy_2O_3 addition is at high fields. This suggests that while in principle some pinning from nanoprecipitates might be expected, the high-field J_cs are mainly driven by

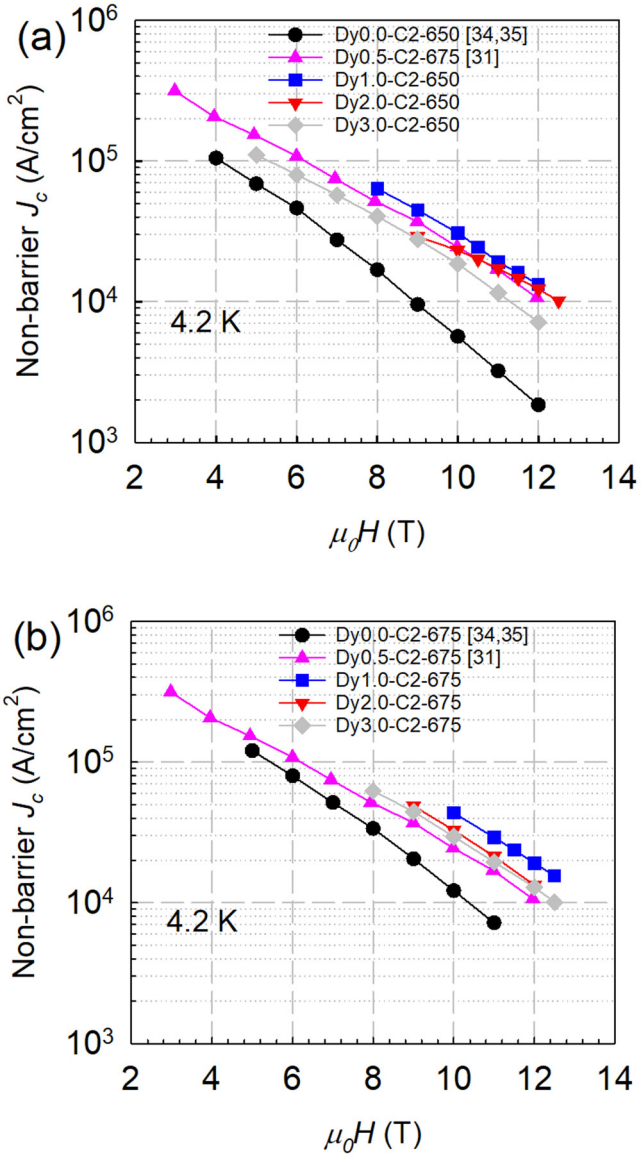

FIG. 1. Field dependence of transport non-barrier J_cs for the samples HT with (a) 650 °C/1h and (b) 675 °C/2h. Non-barrier J_cs of samples Dy0.0-C2-650 from Refs. 34 and 35, Dy0.0-C2-675 from Refs. 34 and 35, and Dy0.5-C2-675 from Ref. 31 are included for comparison.

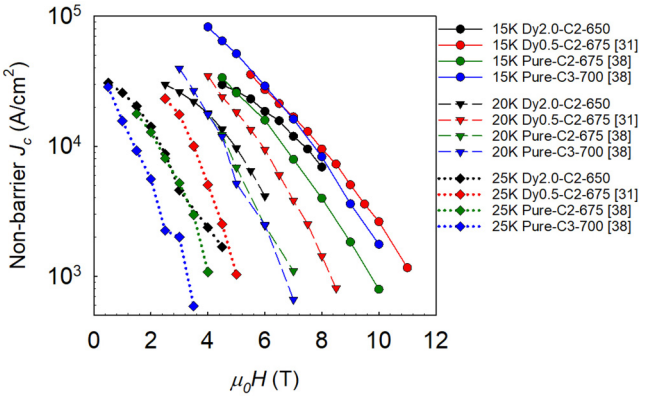

FIG. 2. Comparison for transport non-barrier J_c at 4.2, 15, 20, and 25 K between 2.0 mol. % pure-C-doped sample Pure-C2-675 from Ref. 38, 3.0 mol. % pure-C-doped sample Pure-C3-700 from Ref. 38, 2 mol. % C/2.0 wt. % Dy_2O_3 co-added sample Dy2.0-C2-650 in this study, and 2.0 mol. % C/0.5 wt. % Dy_2O_3 co-added sample Dy0.5-C2-675 from Ref. 31.

increased H_{irr} or H_{c2}. Of course, we could perhaps increase H_{c2} with further C additions. We can then compare the J_c–$\mu_0 H$ data for higher C-doped samples with the samples that had both Dy_2O_3 and 2 mol. % C both at 4.2 K as well as at higher temperatures. To this end, Fig. 2 compares the transport non-barrier $J_c(\mu_0 H)$ of sample Dy2.0-C2-650 in this study and Dy0.5-C2-675 from Ref. 31 with the MgB_2 samples with 2.0 and 3.0 mol. % C doping from Ref. 38, which are labeled as Pure-C2-675 and Pure-C3-700 from 4.2 to 25 K. At 20 K/5 T, sample Dy0.5-C2-675 with co-addition of 0.5 wt. % Dy_2O_3 generated transport J_c of 1.80×10^4 A/cm^2 from Ref. 31 and sample Dy2.0-C2-675 with co-addition of 2.0 wt. % Dy_2O_3 generated 9.65×10^3 A/cm^2 compared to 6.92×10^3 A/cm^2 for 2.0 mol. % C doping and 5.00×10^3 A/cm^2 for 3.0 mol. % C doping from Ref. 38.

Compared to sample Pure-C2-675, although sample Pure-C3-700 has higher non-barrier J_cs at 15 K, Pure-C3-700 has similar 20 K J_cs and obtained an even smaller 25 K J_cs at all applied fields, with respect to the 2 mol. % C sample. Thus, for C-doped samples, 3.0 mol. % C doping is best below 20 K, and 2.0 mol. % C doping is best above 20 K. Bringing in now Dy2.0-C2-650 to the comparison, it meets the performance of the Pure-C3-700 sample at 15 K and outperforms both C only doped chemistries at 20 and 25 K. Finally, Dy0.5-C2-675 outperforms all other samples at 20 and 25 K. These results indicate that Dy_2O_3 co-doping with 2 mol. % C co-addition is a more effective way to improve J_c than heavier C doping over a wide temperature range. At higher temperatures, the lighter Dy_2O_3 doping is better.

B. Upper critical fields and irreversibility fields

Figure 3(a) shows examples of $R(\mu_0 H)$ curves from which values of $\mu_0 H_{c2}$ and $\mu_0 H_{irr}$ were extracted at 4.2 K for Dy0.0-C2-675 and Dy1.0-C2-675. For each sample, two $R(\mu_0 H)$ curves were obtained by first increasing $\mu_0 H$ from 0 to 30 T and then decreasing it from 30 to 0 T. $\mu_0 H_{c2}$(4.2 K) is the average value of $\mu_0 H_{c2}$s extracted from two $R(\mu_0 H)$ curves, and same averaging was applied to $\mu_0 H_{irr}$(4.2 K). Figure 3(b) displays $\mu_0 H_{c2}$ and $\mu_0 H_{irr}$ vs T for Dy0.0-C2-675 and Dy1.0-C2-675. Little difference is seen at 15 K and above, but $\mu_0 H_{c2}$(4.2 K) and $\mu_0 H_{irr}$(4.2 K) are indeed increased by 2.29 and 2.85 T by the 1.0 wt. % Dy_2O_3 addition, respectively. Here, we have used a resistive method to obtain $\mu_0 H_{irr}$. However, in some studies, the irreversibility field is defined at the point where J_c reaches 10^3 A/cm^2, we have denoted the irreversibility field extracted in this alternative way $\mu_0 H_{irr}$*. Table I gives the

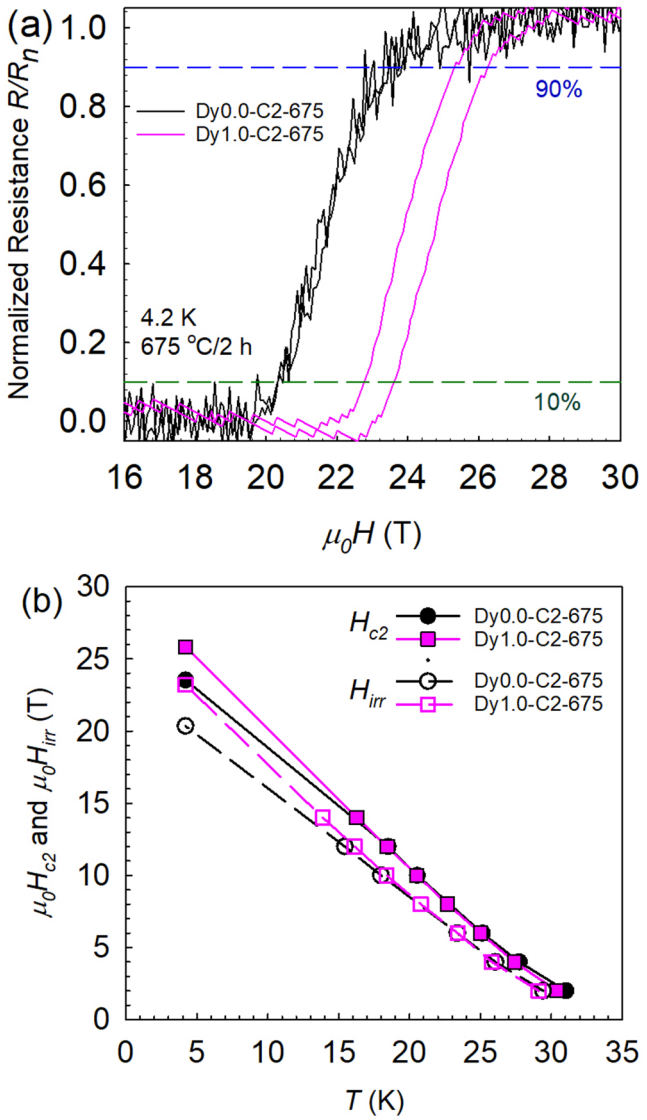

FIG. 3. (a) R-$\mu_0 H$ curves of Dy0.0-C2-675 and Dy1.0-C2-675 at 4.2 K. (b) $\mu_0 H_{c2}$ and $\mu_0 H_{irr}$ as a function of temperature for samples Dy0.0-C2-675 and Dy1.0-C2-675.

values for $\mu_0 H_{irr}$* for Dy2.0-C2-650, Pure-C2-675, and Pure-C3-700. It can be seen that H_{irr}* is suppressed at higher temperatures by increasing the C concentration from 2 to 3 mol. %. However, the C/Dy_2O_3 co-addition generates a larger H_{irr}* than 2 mol. % C doping at all temperatures, even though the enhancements are more pronounced at lower temperatures.

C. Anisotropy and $H_{c2//c}$

The above results indicate that 4.2 K H_{c2} (=$H_{c2//ab}$) is increased by Dy_2O_3/C co-addition, while no increase is seen at higher temperatures. On the other hand, H_{irr} (or H_{irr}*), which is correlated to $H_{c2//c}$, is increased over a larger range of temperatures, even though the largest increases are seen at low fields. Eisterer's percolation model for MgB_2 allows us to extract the values of $H_{c2//c}$ from H_{irr} using the following relationship connecting measured H_{c2} (=$H_{c2//ab}$), γ (and thus $H_{c2//c}$), and an effective percolation threshold p_c* with a fixed number:[39–41]

TABLE I. Comparison of $\mu_0 H_{irr}$* (Unit: T) between Pure-C3-700, Pure-C2-675, and Dy2.0-C2-650.

Temperature (K)	Dy2.0-C2-650	Pure-C3-700[a]	Pure-C2-675[a]
4.2	19.1	21.6	15.9
15	12.2	11.1	9.70
20	8.01	6.92	7.00
25	5.01	3.28	4.00

[a]$\mu_0 H_{irr}$*s of Pure-C3-700 and Pure-C2-675 are extracted from non-barrier $J_c(\mu_0 H)$ curves from Ref. 38.

$$\Delta T = \frac{1-\sqrt{(\gamma^2-1)p_c^{*2}+1}}{dH_{c2}/dT} H. \quad (1)$$

This indicates that $H_{c2//c}$, while not directly measurable in polycrystalline samples, is directly proportional to H_{irr}. That is, H_{irr} and $H_{c2//c}$ are directly tied together, with H_{irr} being slightly different with $H_{c2//c}$ by an amount related to a percolation effect. The essence of the model is that a certain number of grains, which are, in principle, randomly oriented with respect to the applied field, are required to be superconducting in order for a superconducting path to be continuous. As field or temperature is decreased from the normal state, more and more lengths along a given path are contiguous, until at H_{irr}, a complete path exists. The percolation model describes not only the nature of resistive transition, but also influences the form of J_c vs $\mu_0 H$, given as[39–41]

$$J_c(\alpha) = F_0 \frac{[1-H/H_{c2}(\alpha)]^2}{\mu_0 \sqrt{H H_{c2}(\alpha)}}, \quad (2)$$

where $J_c(\alpha)$ is the microscopic J_c dominated by grain-boundary flux pinning, F_0 is the pinning strength, and α represents the angle between the magnetic field and the c-axis of MgB_2 grain. Then, macroscopic J_c of polycrystalline MgB_2 can be given as[39–41]

$$\begin{aligned} J_c &= \int_0^{J_c^{max}(\mu_0 H)} \left(\frac{p_{MgB_2} p(J) - p_c}{1-p_c}\right)^{1.79} dJ \\ &= \int_0^{J_c^{max}(\mu_0 H)} \left(\frac{p_{MgB_2} - p_c}{1-p_c}\right)^{t} \left(\frac{p(J) - p_c/p_{MgB_2}}{1-p_c/p_{MgB_2}}\right)^{1.79} dJ \\ &= \int_0^{J_c^{max}(\mu_0 H)} A_{con} \left(\frac{p(J) - p_c^*}{1-p_c^*}\right)^{1.79} dJ, \end{aligned} \quad (3)$$

where $p(J)$ is the fraction of superconducting grains whose $J_c(\alpha)$ is larger than J, $p(MgB_2)$ is the fraction of MgB_2 grains in the polycrystalline sample, $p_c = p(MgB_2) \times p_c^*$ is percolation threshold, $J_c^{max}(\mu_0 H)$ is defined as $p[J_c^{max}(\mu_0 H)]$ that is equal to p_c, and the values of p_c and t are determined to be 0.17–0.31 and 1.79, respectively.[39] Thus, four parameters (F_m, $\mu_0 H_{c2}$, γ, and p_c^*) are required for obtaining best fitting of transport J_c using the percolation model and $F_m = F_0 \times A_{con}$ is the effective flux pinning strength. For Dy0.0-C2-675 and Dy1.0-C2-675, the field dependence of 4.2 K non-barrier J_c has been fit by the percolation model; results are shown in Fig. 4. The 4.2 K values of $\mu_0 H_{c2}$ ($=\mu_0 H_{c2//ab}$) for Dy0.0-C2-675 and Dy1.0-C2-675 were measured and were used in the fitting of Fig. 4 and listed in Table II. Table II also gives the values of other fitting parameters, and the calculated values for $\mu_0 H_{c2//c}$. p_c^* are assumed to be fixed at 0.2 for simplicity. In some cases, the samples transitioned by quench, but this was interpreted as J_c for present purposes (previous work has shown these values to be very close to the critical surface). The effective flux pinning strength of 1.0 wt. % reaches 4.12×10^6 A T cm^{-2}, which is 51% higher than that of 0.0 wt. % wire. This result confirms previous reports that Dy_2O_3 additions increase flux pinning.[27] More interesting, however, is that Dy_2O_3 addition decreases the anisotropy γ. The 4.2 K γ of Dy0.0-C2-675 is 2.52, but 1 wt. % addition of Dy_2O_3 decreases γ to 2.14. The 4.2 K $\mu_0 H_{c2//c}$ for Dy0.0-C2-675 and Dy1.0-C2-675 are calculated to be 9.34 T and 12.30 T, respectively. Consequently, the Dy_2O_3 addition can further increase both $H_{c2//c}$ and $H_{c2//ab}$ for C-doped MgB_2 at 4.2 K, and provides a stronger enhancement of $H_{c2//c}$ than $H_{c2//ab}$.

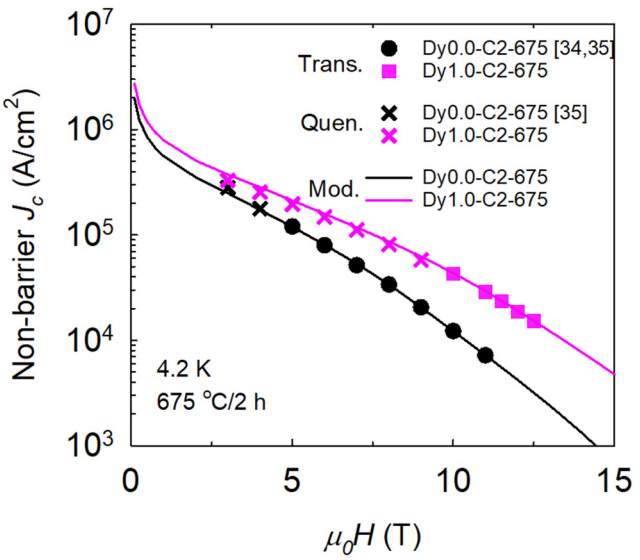

FIG. 4. Experimental transport non-barrier J_cs (solid dots), quench Js (cross dots), and modeling J_cs (solid lines) for Dy0.0-C2-675 and Dy1.0-C2-675. Transport non-barrier J_cs of Dy0.0-C2-675 are from Ref. 34 and 35. Quench Js of Dy0.0-C2-675 are from Ref. 35.

TABLE II. List of fitting parameters for the percolation model and calculated $\mu_0 H_{c2//c}$ at 4.2 K.

Fitting Parameter	Dy0.0-C2-675	Dy1.0-C2-675
F_m (A T cm^{-2})	2.73×10^6	4.12×10^6
Anisotropy, γ	2.52	2.14
$\mu_0 H_{c2}$ ($=\mu_0 H_{c2//ab}$) (T)	23.5	26.3
$\mu_0 H_{c2//c}$ (T)	9.34	12.3

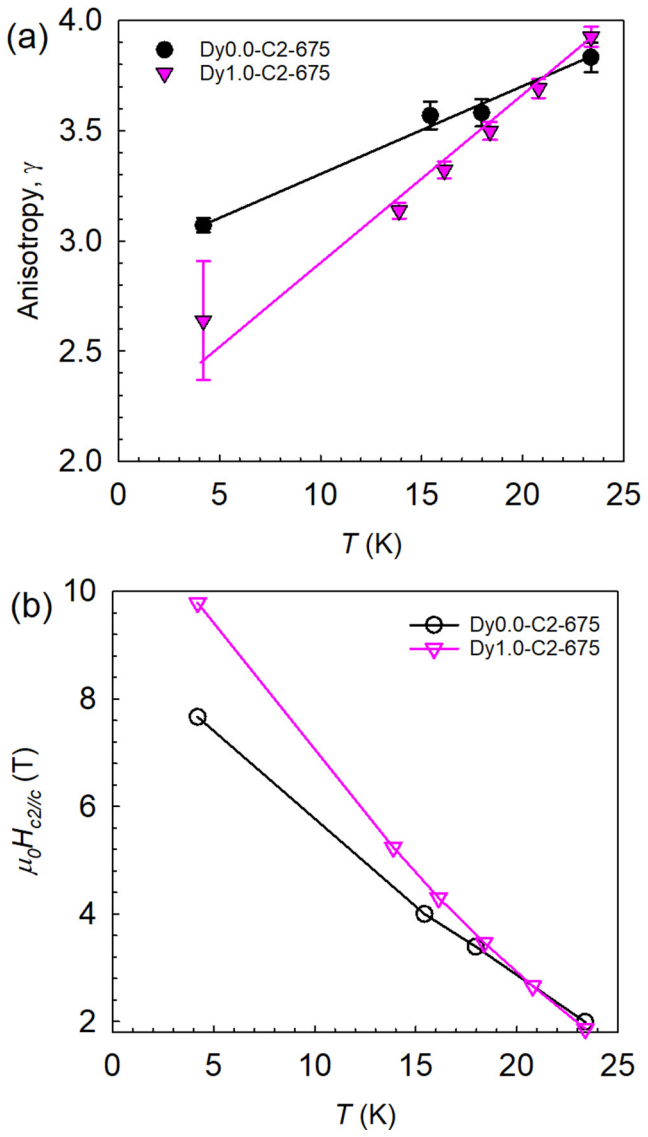

FIG. 5. Temperature dependence of (a) anisotropy γ and (b) $\mu_0 H_{c2//c}$ for Dy0.0-C2-675 and Dy1.0-C2-675.

The 1.0 wt. % Dy_2O_3 addition tends to decrease anisotropy γ at temperatures $\lesssim$20 K and correspondingly enhances $H_{c2//c}$, Fig. 5. The values of γ are calculated for both Dy1.0-C2-675 and Dy0.0-C2-675 using Eq. (1). The γ value of 3.8 at 23.4 K for Dy0.0-C2-675 is similar to that of C-doped MgB_2 reported by Eisterer,[42] for which $\gamma = 4$ at 21 K as the T_c of C-doped MgB_2 is 35 K. Anisotropy γ grows with temperature for both samples due to anisotropic σ bands determining γ at high temperatures while isotropic π bands define γ at low temperatures.[43] It has been reported that, without $H_{c2//ab}$ enhancement, adding 0.5 wt. % Dy_2O_3 enhances H_{irr} for C-doped MgB_2.[31] Based on present results, the H_{irr} enhancement can be considered as a result of $H_{c2//c}$ enhancement or decrease in γ caused by Dy_2O_3 addition. Nevertheless, the increases in $H_{c2//ab}$ and $H_{c2//c}$ are not pronounced at high temperatures. In any case, it is of interest to explore further the $H_{c2//ab}(T)$ and $H_{c2//c}(T)$ behaviors as influenced by Dy_2O_3 addition. To do this, we will model $H_{c2//ab}$ and $H_{c2//c}$ values extracted above using the two band, anisotropic model for MgB_2.

IV. DISCUSSION

According to Gurevich's discussion,[1,43] H_{c2} is related to electronic diffusivities (D_σ and D_π) associated with σ and π bands, respectively. Associated with the anisotropy of MgB_2, D_σ and D_π also have an angular dependence, which can be given as

$$D_n(\alpha) = \sqrt{(D_n^{ab})^2\cos^2(\alpha) + (D_n^{ab})(D_n^{c})\sin^2(\alpha)}, \tag{4}$$

where α represents the angle between the direction of the applied field and the c-axis of the MgB_2 lattice and D_n^{ab} and D_n^{c} are electronic diffusivities in the ab-plane and c-axis (again index n corresponds to the π or σ band), respectively. Thus, we have given an expression for the effective diffusivity in a plane perpendicular to α, using the defined electronic diffusivities for each band along a given direction within the crystal. In this case, the limiting cases of $D_n(\pi/2)$ and $D_n(0)$ can be expressed as

$$D_n(0) = D_n^{ab} \tag{5}$$

and

$$D_n(\pi/2) = \sqrt{D_n^{ab}D_n^{c}}. \tag{6}$$

The electronic diffusivities, D_σ and D_π, represent the degree of intraband scattering for MgB_2 conductor and decreased D_σ and D_π are the reflection of increased intraband scattering rates caused by impurity doping/addition. While the $H_{c2}(T)$ behavior of MgB_2 is affected by both intraband scattering rates as well as interband scattering rates, parametrized by $\Gamma_{\pi\sigma}$ and $\Gamma_{\sigma\pi}$, and T_c is also correlated with interband scattering. In Gurevich's two-gap dirty limit theory, the effects of intra- and interband scattering on the H_{c2} of a two-gap MgB_2 having a σ band and a π band can be described by linearized Usadel equations,[1,44]

$$\omega f_\sigma - \frac{D_\sigma}{2}\Pi^2 f_\sigma = \Delta_\sigma + (f_\pi - f_\sigma)\Gamma_{\sigma\pi}, \tag{7}$$

$$\omega f_\pi - \frac{D_\pi}{2}\Pi^2 f_\pi = \Delta_\pi + (f_\sigma - f_\pi)\Gamma_{\pi\sigma}, \tag{8}$$

where $f_{\sigma,\pi}$ is the Usadel green function associated with the σ or π band, ω is the Matsubara frequency, $D_{\sigma,\pi}$ is the intraband diffusivity due to intraband scattering in either σ or π band, $\Gamma_{\sigma\pi}$ and $\Gamma_{\pi\sigma}$ are interband scattering rates, and $\Delta_{\sigma,\pi}$ is the σ or π bandgap. Then, for a two-gap MgB_2 conductor, the solution to the linearized Usadel equations for the condition $T = T_c$ can be expressed as[1,43]

$$U\left(\frac{g}{t_c}\right) = \psi\left(\frac{1}{2}+\frac{g}{t_c}\right) - \psi\left(\frac{1}{2}\right) = -\frac{\ln t_c(w\ln t_c + \lambda_0)}{w\ln t_c + p}, \tag{9}$$

where $t_c = T_c/T_{c0}$, $g = (\Gamma_{\sigma\pi} + \Gamma_{\pi\sigma})\hbar/(2\pi k_B T_{c0})$ is called the interband scattering parameter, T_c is the critical temperature of MgB_2 due to interband scattering, and T_{c0} is the critical temperature of MgB_2 without interband scattering ($\Gamma_{\sigma\pi} = \Gamma_{\pi\sigma} = 0$). Here, $\psi(x)$ is the di-gamma function, while W, λ_0, and p are appropriate functions of interband scattering rates and BSC coupling constants of $\lambda_{\sigma\sigma} = 0.810$, $\lambda_{\sigma\pi} = 0.119$, $\lambda_{\pi\sigma} = 0.09$, and $\lambda_{\pi\pi} = 0.285$, which is given by[1,44–46]

$$w = \lambda_{\sigma\sigma}\lambda_{\pi\pi} - \lambda_{\sigma\pi}\lambda_{\pi\sigma}, \tag{10}$$

$$\lambda_- = \lambda_{\sigma\sigma} - \lambda_{\pi\pi}, \tag{11}$$

$$\lambda_0 = (\lambda_-^2 + 4\lambda_{\sigma\pi}\lambda_{\pi\sigma})^{1/2}, \tag{12}$$

$$\Gamma_\pm = \Gamma_{\sigma\pi} \pm \Gamma_{\pi\sigma}, \tag{13}$$

$$2p = \lambda_0 + [\Gamma_-\lambda_- - 2\lambda_{\sigma\pi}\Gamma_{\pi\sigma} - 2\lambda_{\pi\sigma}\Gamma_{\sigma\pi}]/\Gamma_+. \tag{14}$$

Equation (9) demonstrates the relationship between g, T_c, and interband scattering rates. On the other hand, for the condition of $H = H_{c2}$, the solution to the linearized Usadel equations can be expressed as[1]

$$2w(\ln t + U_+)(\ln t + U_-) + (\lambda_0 + \lambda_i)(\ln t + U_+) + (\lambda_0 - \lambda_i)(\ln t + U_-) = 0, \tag{15}$$

where $t = T/T_{c0}$, $U_\pm = \psi(1/2 + \hbar\Omega_\pm/(2\pi k_B T)) - \psi(1/2)$, $\Omega_\pm$ are the function of $D_{\pi,\sigma}$, $\Gamma_{\sigma\pi}$, $\Gamma_{\pi\sigma}$, and H_{c2} and can be expressed as

$$2\Omega_\pm = \omega_+ + \Gamma_+ \pm \Omega_0, \tag{16}$$

$$\Omega_0 = (\omega_-^2 + \Gamma_+^2 + 2\Gamma_-\omega_-)^{1/2}, \tag{17}$$

$$\omega_\pm = (D_\sigma \pm D_\pi)\pi\mu_0 H_{c2}/\varnothing_0, \tag{18}$$

$$\lambda_i = [(\omega_- + \Gamma_-)\lambda_- - 2\lambda_{\sigma\pi}\Gamma_{\pi\sigma} - 2\lambda_{\pi\sigma}\Gamma_{\sigma\pi}]/\Omega_0, \tag{19}$$

where $\varnothing_0$ is the flux quantum. Therefore, Gurevich's two-gap dirty limit theory builds a quantitative relationship between H_{c2}, T_c, and intra- and interband scattering for two-gap MgB_2.

Pure MgB_2 has relatively low critical fields, which leads to J_c values that drop off relatively quickly with increasing applied magnetic field. Up until now, the most effective way to increase H_{c2}s of MgB_2 at 4.2–20 K is through the C substitution into the B sublattice, which leads to the increase in intraband scattering rates (smaller $D_{\pi,\sigma}$). Gurevich's two-gap dirty limit theory indicates that the π bands are much dirtier than σ bands for C-doped MgB_2 conductors ($D_\pi \ll D_\sigma$).[1,44,45] However, the H_{c2} of MgB_2 is decreased at relatively high temperatures (≥20 K) if heavy C doping is used; this leads to a corresponding decrease in J_cs at high temperatures. For example, although the J_cs of powder-in-tube *in situ* MgB_2 wires are improved at 4.2 K by increasing C doping from 2.0 to 3.0 mol. %, the J_cs are suppressed at 25 K.[32,38] These results are induced by the fact that heavy C doping increases interband scattering rates, which is reflected in a decrease in T_c.

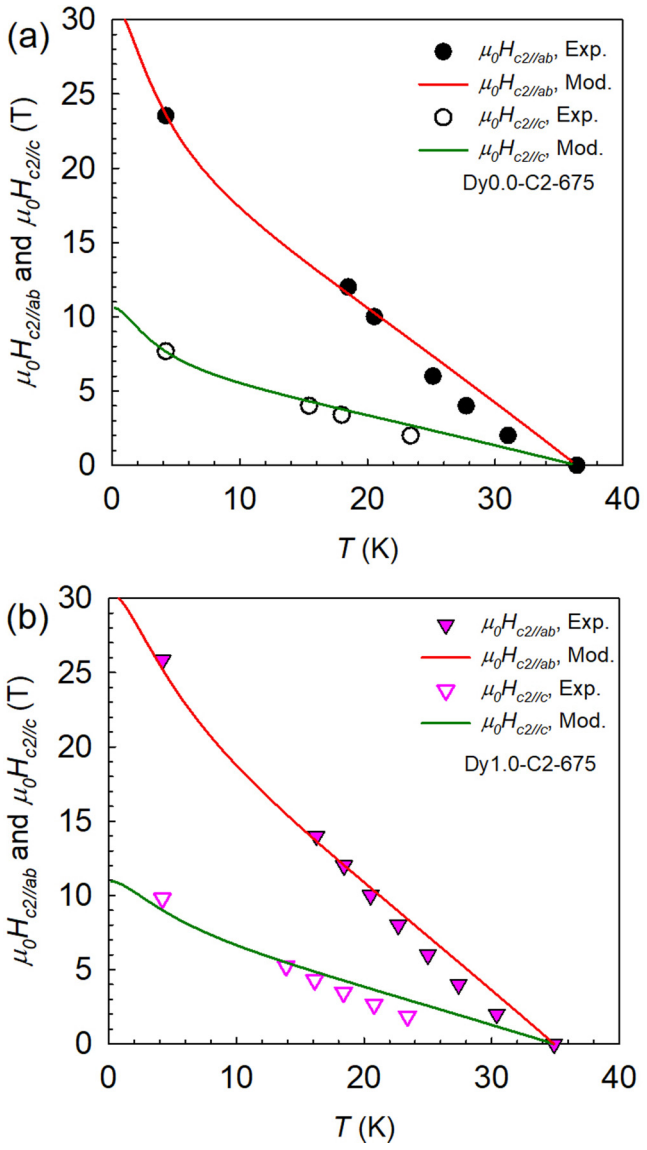

FIG. 6. Temperature dependence of $\mu_0H_{c2//ab}$ and $\mu_0H_{c2//c}$ and fitting curves for (a) Dy0.0-C2-675 and (b) Dy1.0-C2-675.

The T_cs of Dy0.0-C2-675 and Dy1.0-C2-675 are measured to be 36.4 and 34.9 K, respectively, and the g values of the samples are solved to be 0.054 and 0.081 using Eq. (11). Once the values of g are known, the values of interband scattering rates, $\Gamma_{\sigma\pi}$ and $\Gamma_{\pi\sigma}$, can be calculated by solving the simultaneous equations of $N_\sigma\Gamma_{\sigma\pi} = N_\pi\Gamma_{\pi\sigma}$, $N_\pi \approx 1.3N_\sigma$, and $g = (\Gamma_{\sigma\pi} + \Gamma_{\pi\sigma})\hbar/(2\pi k_B T_{c0})$. Then, by inserting the values of $\Gamma_{\sigma\pi}$ and $\Gamma_{\pi\sigma}$ into Eqs. (15)–(19), μ_0H_{c2} can be treated as the solution to Eq. (15) for certain values of T, D_σ, and D_π. In other words, the curve of μ_0H_{c2} vs T can be modelled by setting the values of D_σ and D_π if the values of $\Gamma_{\sigma\pi}$ and $\Gamma_{\pi\sigma}$ are known. Figure 6 shows $\mu_0H_{c2//ab}$ and $\mu_0H_{c2//c}$ vs T for Dy0.0-C2-675 and Dy1.0-C2-675. Also shown is a fit based on Gurevich's two-gap dirty limit theory and the fitting parameters are listed in Table III. The fitting parameters of $(D_\sigma^{ab}D_\sigma^c)^{1/2}$ were used to calculate $H_{c2//ab}$, and $H_{c2//c}$ is associated with the values of D_σ^{ab}. Since the π band is more isotropic than the σ band, $D_\pi^{ab}/D_\pi^c \sim 1$ and $D_\sigma^c \ll D_\sigma^{ab}$,[1,47,48] the fitting parameter of D_π representing $(D_\pi^{ab}D_\pi^c)^{1/2}$, D_π^{ab}, and D_π^c($D_\pi = D_\pi^{ab} = D_\pi^c = (D_\pi^{ab}D_\pi^c)^{1/2}$) was used to fit the data of $\mu_0H_{c2//ab}(T)$ and $\mu_0H_{c2//c}(T)$. At higher temperatures, the experimental values of both $H_{c2//ab}$ and $H_{c2//c}$ are lower than the theoretical curves for both samples. This could be due to an increase in p_c with temperature (due to C or Dy_2O_3 accumulation at the grain boundaries and related "inhomogeneities") as suggested by Eisterer.[39] According to Eq. (1), the increase in p_c with temperature induces ΔT_c broadening of ρ–T curves in superconductors at high temperatures. Moreover, ΔT_c broadening at high temperature can also be caused by thermal fluctuations.[39] Both $H_{c2//ab}(T)$ and $H_{irr}(T)$ extracted from ρ–T curves with ΔT_c broadening are smaller than those extracted from ρ–T curves without ΔT_c broadening, as they correspond to 90% and 10% of the normal state, respectively. Since $H_{c2//c}$ is associated with H_{irr}, $H_{c2//c}$ is also underestimated due to ΔT_c broadening at high temperatures. The difference between our H_{c2} fitting parameters, D_σs, with those obtained by Refs. 49 and 50 is within 40%. Since our H_{c2} fitting follows the rule that π bands are isotropic ($D_\pi = D_\pi^{ab} = D_\pi^c$), our D_π value is comparable to only one of D_πs reported by Refs. 49 and 50.

In the first place, it can be seen that Dy_2O_3 addition do increase g and also decrease $(D_\sigma^{ab}D_\sigma^c)^{1/2}$, D_σ^{ab}, and D_π further for already C-doped MgB_2. In other words, both intraband and interband scattering rates of C-doped MgB_2 are increased by adding Dy_2O_3. We note that Dy_2O_3 additions, unlike C and Al doping, are unable to induce B or Mg-site substitution within the MgB_2 lattice.

TABLE III. Parameters for fitting $\mu_0H_{c2//ab}$(T) and $\mu_0H_{c2//c}$(T) curves and calculated D_σ^{ab} and D_σ^c.

Fitting parameter	Dy0.0-C2-675	Dy1.0-C2-675
g	0.054	0.081
$(D_\sigma^{ab}D_\sigma^c)^{1/2}$(cm²/s)	1.73	1.59
D_σ^{ab}(cm²/s)	5.45	4.50
$D_\pi = D_\pi^{ab} = D_\pi^c$(cm²/s)	0.0172	0.0100

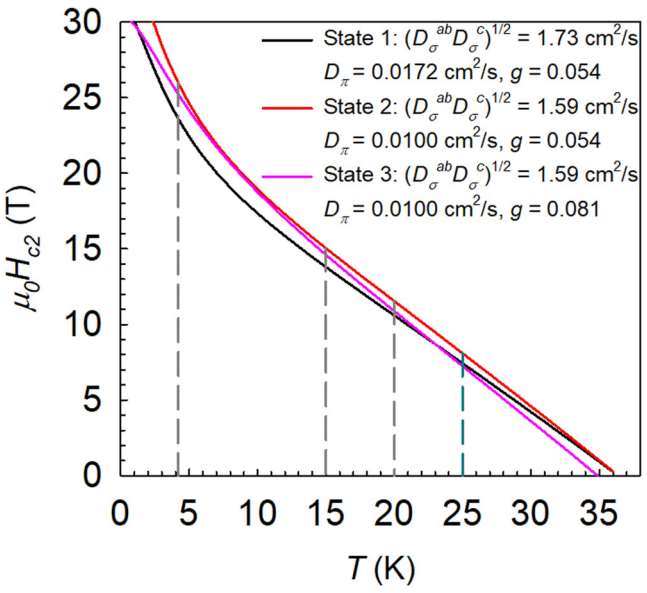

FIG. 7. Effects of $(D_\sigma^{ab}D_\sigma^{c})^{1/2}$, D_π, and g on $\mu_0 H_{c2//ab}$(T) behavior of MgB_2. State 1 represents the performance of $(D_\sigma^{ab}D_\sigma^{c})^{1/2} = 1.73\,cm^2/s$, $D_\pi = 0.0172\,cm^2/s$, and $g = 0.054$. State 2 represents the performance of $(D_\sigma^{ab}D_\sigma^{c})^{1/2} = 1.59\,cm^2/s$, $D_\pi = 0.0100\,cm^2/s$, and $g = 0.054$. State 3 represents the performance of $(D_\sigma^{ab}D_\sigma^{c})^{1/2} = 1.59\,cm^2/s$, $D_\pi = 0.0100\,cm^2/s$, and $g = 0.081$.

It is also known that secondary phases that collect within the grain boundaries can increase $\mu_0 H_{c2//ab}$.[51] However, given the fact that DyB_4 nanoinclusions are known to form within the grains and that we see increases in both $\mu_0 H_{c2//ab}$ and $\mu_0 H_{irr}$, the most probable mechanism for the increase in band scattering is that DyB_4 nanoinclusions[27,31] have short-range localized strain in the MgB_2 matrix. The effects of Dy_2O_3 additions can be separated into two states. First, the properties $[(D_\sigma^{ab}D_\sigma^{c})^{1/2} = 1.73\,cm^2/s,\ D_\pi = 0.0172\,cm^2/s,\ g = 0.054]$ of Dy0.0-C2-675 are set as starting points, which is called state 1. Then, the influence of 1.0 wt. % Dy_2O_3 addition on intraband scattering is accounted for, which leads to a transition from state 1 to state 2 by decreasing the values of $(D_\sigma^{ab}D_\sigma^{c})^{1/2}$ and D_π to 1.59 and $0.0100\,cm^2/s$, respectively. Next, increasing the value of g to 0.081 accounts for the influence of 1.0 wt. % Dy_2O_3 addition on the interband scattering effect, leading to a transition from state 2 to state 3. Figure 7 shows the change of $\mu_0 H_{c2//ab}$(T) caused by the whole set of transitions from state 1 to state 2 to state 3. Decreasing $(D_\sigma^{ab}D_\sigma^{c})^{1/2}$ from 1.73 to $1.59\,cm^2/s$ and D_π from 0.0172 to $0.0100\,cm^2/s$ induces $H_{c2//ab}$ enhancements, leading to a $\Delta\mu_0 H_{1\to2}$ of +2.357 T at 4.2 K, +1.245 T at 15 K, +0.949 T at 20 K, and +0.663 T at 25 K, as shown in Table IV. By keeping $(D_\sigma^{ab}D_\sigma^{c})^{1/2} = 1.59\,cm^2/s$ and $D_\pi = 0.0100\,cm^2/s$ unchanged,

TABLE IV. Comparison of $\mu_0 H_{c2}$ (unit: T) for state 1, state 2, and state 3 in Fig. 7. $\Delta\mu_0 H_{1\to2}$ and $\Delta\mu_0 H_{2\to3}$ represent the transitions from state 1 to state 2 and from state 2 to state 3, respectively. $\Delta\mu_0 H$ is the sum of $\Delta\mu_0 H_{1\to2}$ and $\Delta\mu_0 H_{2\to3}$.

T (K)	$\mu_0 H_{c2}$ in state 1	$\mu_0 H_{c2}$ in state 2	$\Delta\mu_0 H_{1\to2}$	$\mu_0 H_{c2}$ in state 3	$\Delta\mu_0 H_{2\to3}$	$\Delta\mu_0 H$
4.2	23.54	25.89	+2.357	25.17	−0.727	+1.630
15	13.80	15.05	+1.245	14.61	−0.431	+0.814
20	10.59	11.54	+0.949	10.88	−0.663	+0.287
25	7.427	8.090	+0.663	7.247	−0.843	−0.180

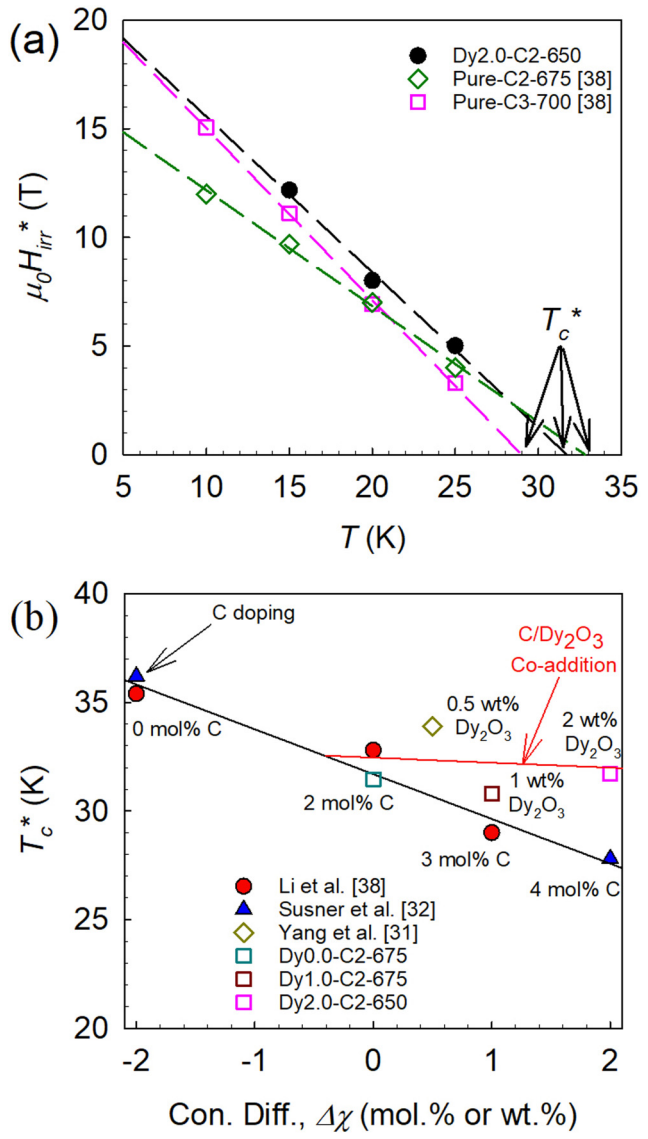

FIG. 8. Comparison of (a) $\mu_0 H_{irr}$*s and T_c* for Dy2.0-C2-650, Pure-C2-675, and Pure-C3-700 and (b) T_c* between C/Dy_2O_3 co-addition and C doping. The H_{irr}*s of Pure-C2-675 and Pure-C3-700 are extracted from the J_c–$\mu_0 H$ data from Ref. 38. The T_c*s are extracted from the $\mu_0 H_{irr}$*–T data from Ref. 38 and $\mu_0 H_{irr}$–T data from Ref. 32 for 0–4 mol. % C doping. The T_c* of 0.5 wt. % Dy_2O_3 are extracted from the $\mu_0 H_{irr}$–T data reported in Ref. 31.

increasing g from 0.054 to 0.081 induces $H_{c2//ab}$ suppression, leading to a $\Delta\mu_0 H_{2\to3}$ of −0.727 T at 4.2 K, −0.431 T at 15 K, −0.663 T at 20 K, and −0.843 T at 25 K. Therefore, adding 1.0 wt. % Dy_2O_3 into already 2 mol. % C-doped MgB_2 causes the change of state 1 → state 2 → state 3, generating a $\Delta\mu_0 H$ ($=\Delta\mu_0 H_{1\to2}+\Delta\mu_0 H_{2\to3}$) of +1.630 T at 4.2 K, +0.814 T at 15 K, +0.287 T at 20 K, and −0.180 T at 25 K, Table IV. Thus, while overall the rate of interband to intraband scattering is lower for Dy_2O_3 than C, allowing Dy_2O_3/C co-doping to lead to higher $H_{c2//c}$ and $H_{c2//ab}$ at elevated temperatures, Dy_2O_3 does have some interband scattering. Thus, heavier 1.0 wt. % Dy_2O_3 addition leads to the small changes in $H_{c2//ab}$ at relatively higher temperatures.

Increased values of g tend to reduce H_{c2}, H_{irr}, and H_{irr}^* at higher temperatures (≥20 K). Such an increase in g can be reflected by a decrease in T_c. In this study, a parameter T_c^* is introduced as a surrogate for T_c. It is defined as the temperature where H_{irr}^* vs T curve extrapolates to zero, Fig. 8(a). When $\mu_0 H_{irr}^*$–T data are not available, similar effective T_c^*s can be obtained by linearly extrapolating $\mu_0 H_{irr}$ vs T curves to zero. The influence of C doping alone as well as C/Dy_2O_3 co-addition on T_c^* can be clarified by setting 2 mol. % C concentration as a reference, as is shown in Fig. 8(b). Here, a concentration difference, $\Delta\chi$, is defined and obtained by subtracting the 2 mol. % from doping or co-addition. Therefore, for samples that only have C doping, $\Delta\chi$ = X − 2 mol. % corresponds to X mol. % C doping. Since the concentration of 2 mol. % C/Y wt. % Dy_2O_3 co-addition can be expressed as (2 mol. % + Y wt. %), the $\Delta\chi$ of this co-addition is Y wt. %. For example, the $\Delta\chi$ of 2.0 wt. % corresponds to 2.0 mol. % C/2.0 wt. % Dy_2O_3 co-addition. As shown in Fig. 8(b), as compared to C/Dy_2O_3 co-addition, C doping decreases T_c^* at a much faster rate, producing a stronger interband scattering and hence greater suppressed H_{c2}/H_{irr} at high temperatures. The overall results indicate that Dy_2O_3/C co-addition is more promising than C doping for seeking better performances of MgB_2 over a wide temperature range.

V. CONCLUSIONS

This study confirms that Dy_2O_3 additions can further increase H_{c2} and H_{irr} of already optimally C-doped MgB_2 at 4.2 K. However, this study goes further, systematically showing the effect of Dy_2O_3 addition on J_cs, $\mu_0 H_{c2}$s, $\mu_0 H_{irr}$s, critical field anisotropies of C-doped PIT MgB_2 wires fabricated with 2 mol. % C doping and co-addition of 0–3 wt. % Dy_2O_3. Irreversibility fields ($\mu_0 H_{irr}$), upper critical fields ($\mu_0 H_{c2}$), and transport critical currents were measured, and from these quantities, the anisotropies (γ) and intraband diffusivities ($D_{\pi,\sigma}$) were estimated for the first time for wires with C and Dy_2O_3 co-additions. The results were compared to previous results for wires with C doping only, and further band scattering, primarily intra-band scattering, was observed due to Dy_2O_3 additions. The highest 4.2 K, 10 T non-barrier J_c of 4.35×10^4 A/cm^2 was achieved by an MgB_2 wire with 1.0 wt. % Dy_2O_3 addition (to 2.0 mol. % C-doped strands) indicating 1.0 wt. % is the optimal Dy_2O_3 concentration (for co-doping with 2.0 mol. % C) for maximizing the non-barrier J_cs of the MgB_2 wire at 4.2–15 K. Above 15 K, we found that 0.5 wt. % Dy_2O_3 doping with 2.0 mol. % C performs better, but in general, Dy_2O_3 + C doping outperforms C-doped-only samples comparing our results in this present work to previous studies. This is because the increases in intraband scattering induced by Dy_2O_3 addition generates lower electronic diffusivities and thus leads to further increased values of H_{irr}^*, H_{irr}, $H_{c2//ab}$, and $H_{c2//c}$ for C-doped MgB_2. The $\mu_0 H_{c2}$ modeling based on the two-band theory shows that the increases in H_{irr}, $H_{c2//ab}$, and $H_{c2//c}$ primarily resulted from the increases in intraband scattering with Dy_2O_3 additions. Thus, C/Dy_2O_3 as co-additives have the potential to obtain higher H_{irr}s than C dopant as C/Dy_2O_3 co-addition increases interband scattering at a lower rate than C doping does, suggesting that C/Dy_2O_3 co-additions are a better approach for improving non-barrier J_c of MgB_2 at higher temperatures.

ACKNOWLEDGMENTS

This work was supported by the NIH, specifically the National Institute of Biomedical Imaging and Bioengineering, under Grant No. R01EB018363. Some of the transport measurements in this work were performed at the NHMFL, which is supported by the U.S. NSF under cooperative Agreement No. DMR-1,644,779, and the state of Florida. The authors are grateful to Dr. Eisterer for providing the MatLab code of MgB_2 percolation.

NOMENCLATURE

D_σ	=	Electronic diffusivity associated with σ band
D_π	=	Electronic diffusivity associated with π band
$D_\sigma(\pi/2)$	=	D_σ for *ab*-plane parallel to the magnetic field
$D_\sigma(0)$	=	D_σ for *c*-axis parallel to the magnetic field
$D_{\sigma,\pi}$	=	Electronic diffusivities due to intraband scattering of σ or π band
D_σ^{ab}	=	D_σ along the direction of *ab*-plane
D_σ^{c}	=	D_σ along the direction of *c*-axis
$f_{\sigma,\pi}$	=	Usadel green function associated with σ or π band
F_0	=	Flux pinning strength
F_m	=	Effective pinning strength
g	=	Interband scattering parameter
J_c	=	Critical current density
$J_c(\alpha)$	=	Microscopic critical current density of MgB_2 grain
k_B	=	Boltzmann constant
p_c	=	Percolation threshold
p_c^*	=	Effective percolation threshold that is equal to p_c/p_{MgB_2}
$p(J)$	=	Fraction of superconducting grains whose J_c is larger than J
p_{MgB_2}	=	Fraction of MgB_2 grains in conductor (number of MgB_2 grains over the total number of MgB_2 grains and voids)
R	=	Resistance of MgB_2 wire
R_n	=	Normal state resistance of MgB_2 wire
t	=	Normalized temperature that is defined as T/T_{c0}
t_c	=	Normalized critical temperature that is defined as T_c/T_{c0}

T_c	=	Critical temperature of MgB_2 wire
T_c^*	=	Critical temperature that is extrapolated from data of $\mu_0 H_{irr}$ vs T or $\mu_0 H_{irr}^*$ vs T
T_{c0}	=	Critical temperature of MgB_2 without interband scatterings
$U(x)$	=	The function that is defined as $\psi(1/2+x)-\psi(x)$
$\mu_0 H_{c2}$	=	Upper critical field of MgB_2 wire
$\mu_0 H_{c2//ab}$	=	Upper critical field when the direction of external field is parallel with ab-plane of MgB_2 lattice
$\mu_0 H_{c2//c}$	=	Upper critical field when the direction of external field is parallel with c-axis of MgB_2 lattice
γ	=	H_{c2} anisotropy that is equal to $H_{c2//ab}/H_{c2//c}$
$\mu_0 H$	=	External magnetic field
ρ	=	Resistivity of MgB_2 wire
ρ_n	=	Normal state resistivity of MgB_2 wire
$\mu_0 H_{irr}$	=	Irreversibility field that is extrapolated from data of R vs $\mu_0 H$ or R vs T
$\mu_0 H_{irr}^*$	=	Irreversibility field that is extrapolated from J_c vs $\mu_0 H$
α	=	Angle between magnetic field direction and c-axis
$\Gamma_{\pi\sigma}$ and $\Gamma_{\sigma\pi}$	=	Interband scattering rates
ω	=	Matsubara frequency
$\Delta_{\sigma,\pi}$	=	σ or π bandgap
$\psi(x)$	=	Digamma function
$\lambda_{\sigma\sigma}$ and $\lambda_{\pi\pi}$	=	BSC constants that describe intraband coupling
$\lambda_{\sigma\pi}$ and $\lambda_{\pi\sigma}$	=	BSC constants that describe interband coupling
W, λ_0, λ_-, λ_i and p	=	Appropriate functions of interband scattering rates and BSC coupling constants
$\Omega_\pm$ and Ω_0	=	Appropriate functions of intraband scattering rates, interband scattering rates, and upper critical fields
$\emptyset_0$	=	Flux quantum
$\hbar$	=	Reduced Planck constant
$\Delta\mu_0 H_{1\to2}$	=	$\mu_0 H_{c2//ab}$ of state 2 minus $\mu_0 H_{c2//ab}$ of state 1
$\Delta\mu_0 H_{2\to3}$	=	$\mu_0 H_{c2//ab}$ of state 3 minus $\mu_0 H_{c2//ab}$ of state 2
$\Delta\mu_0 H$	=	Sum of $\Delta\mu_0 H_{1\to2}$ and $\Delta\mu_0 H_{2\to3}$

AUTHOR DECLARATIONS

Conflict of Interest

The authors have no conflicts to disclose.

Author Contributions

F. Wan: Conceptualization (equal); Data curation (lead); Formal analysis (equal); Investigation (equal); Methodology (equal); Software (lead); Writing – original draft (lead); Writing – review & editing (equal). **M. D. Sumption:** Conceptualization (equal); Formal analysis (equal); Funding acquisition (lead); Investigation (equal); Methodology (equal); Project administration (lead); Supervision (equal); Writing – review & editing (equal). **E. W. Collings:** Conceptualization (equal); Formal analysis (equal); Investigation (equal); Supervision (equal); Writing – review & editing (equal).

DATA AVAILABILITY

The data that support the findings of this study are available from the corresponding author upon reasonable request.

REFERENCES

[1] A. Gurevich, Physica C **456**, 160–169 (2007).
[2] J. Kortus, I. I. Mazin, K. D. Belashchenko, V. P. Antropov, and L. L. Boyer, Phys. Rev. Lett. **86**, 4656–4659 (2001).
[3] X. X. Xi, Rep. Prog. Phys. **71**, 116501 (2008).
[4] U. Welp, A. Rydh, G. Karapetrov, W. K. Kwok, G. W. Crabtree, C. Marcenat, L. Paulius, T. Klein, J. Marcuc, K. H. P. Kim, C. U. Jung, H.-S. Lee, B. Kang, and S.-I. Lee, Phys. Rev. B **67**, 012505 (2003).
[5] D. Gajda, A. Morawski, A. J. Zaleski, M. Akdogan, H. Yetis, F. Karaboga, T. Cetner, and I. Belenli, J. Alloys Compd. **687**, 616–622 (2016).
[6] A. Serquis, L. Civale, D. L. Hammon, X. Z. Liao, J. Y. Coulter, Y. T. Zhu, M. Jaime, D. E. Peterson, F. M. Mueller, V. F. Nesterenko, and Y. Gu, Appl. Phys. Lett. **82**, 2847–2849 (2003).
[7] M. S. A. Hossain, S. Senatore, R. Flukiger, M. A. Rindfleisch, and M. J. Tomsic, Supercond. Sci. Technol. **22**, 095004 (2009).
[8] R. Flukiger, M. S. A. Hossain, and C. Senatore, Supercond. Sci. Technol. **22**, 085002 (2009).
[9] M. S. A. Hossain, J. H. Kim, X. Xu, X. L. Wang, M. Rindfleisch, M. Tomsic, M. D. Sumption, E. W. Collings, and S. X. Dou, Supercond. Sci. Technol. **20**, L51–L54 (2007).
[10] S. X. Dou, A. V. Pan, S. Zhou, M. Lonescu, H. K. Liu, and P. R. Munroe, Supercond. Sci. Technol. **15**, 1587–1591 (2002).
[11] S. Soltanian, X. L. Wang, J. Horvat, S. X. Dou, M. D. Sumption, M. Bhatia, E. W. Collings, P. Munroe, and M. Tomsic, Supercond. Sci. Technol. **18**, 658–666 (2005).
[12] S. X. Dou, S. Soltanian, J. Horvat, X. L. Wang, S. H. Zhou, M. Ionescu, and H. K. Liu, Appl. Phys. Lett. **81**, 3419–3421 (2002).
[13] M. D. Sumption, M. Bhatia, S. X. Dou, M. Rindfliesch, M. Tomsic, L. Arda, M. Ozdemir, Y. Hascicek, and E. W. Collings, Supercond. Sci. Technol. **17**, 1180–1184 (2004).
[14] D. Guan, D. Wang, and Y. Ma, Supercond. Sci. Technol. **34**, 115007 (2021).
[15] X. L. Wang, S. Soltanian, M. James, M. J. Qin, J. Horvat, Q. W. Yao, H. K. Yao, and S. X. Dou, Physica C **408–410**, 63–67 (2004).
[16] Y. Ma, X. Zhang, G. Nishijima, K. Watanabe, S. Awaji, and X. Bai, Appl. Phys. Lett. **88**, 072502 (2006).
[17] D. Wang, D. Xu, X. Zhang, C. Yao, P. Yuan, Y. Ma, H. Oguro, S. Awaji, and K. Watanabe, Supercond. Sci. Technol. **29**, 065003 (2016).
[18] D. Wang, Y. Ma, C. Yao, D. Xu, X. Zhang, and S. Awaji, Supercond. Sci. Technol. **30**, 064003 (2017).
[19] X. Zhang, Y. Ma, Z. Gao, D. Wang, L. Wang, W. Liu, and C. Wang, J. Appl. Phys. **103**, 103915 (2008).
[20] X. Zhang, D. Wang, Z. Gao, L. Wang, Y. Qi, Z. Zhang, Y. Ma, S. Awaji, G. Nishijima, K. Watanabe, E. Mossang, and X. Chaud, Supercond. Sci. Technol. **23**, 025024 (2010).
[21] D. L. Wang, Y. W. Ma, Z. S. Gao, C. Yao, L. Wang, X. P. Zhang, G. Nishijima, S. Awaji, and K. Watanabe, Physica C **470**, 1435–1437 (2010).
[22] D. Zhang, M. D. Sumption, E. W. Collings, C. J. Thong, and M. A. Rindleisch, Physica C **578**, 1353749 (2020).
[23] Y. Yang, M. A. Susner, M. D. Sumption, M. Rindfleisch, M. Tomsic, and E. W. Collings, IEEE Trans. Appl. Supercond. **22**, 6200110 (2012).

[24]C. Yao, X. Zhang, D. Wang, Z. Gao, L. Wang, Y. Qi, C. Wang, Y. Ma, S. Awaji, and K. Watanabe, Supercond. Sci. Technol. **24**, 055016 (2011).
[25]Z. S. Gao, Y. W. Ma, D. L. Wang, X. P. Zhang, S. Awaji, and K. Watanabe, Chin. Phys. Lett. **27**, 117401 (2010).
[26]J. Wang, Y. Bugoslavsky, A. Berenov, L. Cowey, A. D. Caplin, L. F. Cohen, J. L. MacManus Driscoll, L. D. Cooley, X. Song, and D. C. Larbalestier, Appl. Phys. Lett. **81**, 2026–2028 (2002).
[27]S. K. Chen, M. Wei, and J. L. MacManus-Driscoll, Appl. Phys. Lett. **88**, 192512 (2006).
[28]C. Cheng and Y. Zhao, Appl. Phys. Lett. **89**, 252501 (2006).
[29]G. Gajda, A. Morawski, R. Diduszko, T. Cetner, M. S. A. Hossain, K. Gruszka, D. Gajda, and P. Przyslupski, J. Alloys Compd. **709**, 473–480 (2017).
[30]Y. Yang, M. D. Sumption, and E. W. Collings, Sci. Rep. **6**, 29306 (2016).
[31]Y. Yang, M. D. Sumption, M. Rindfleisch, M. Tomsic, and E. W. Collings, Supercond. Sci. Technol. **34**, 025010 (2021).
[32]M. A. Susner, Y. Yang, M. D. Sumption, E. W. Collings, M. A. Rindfleisch, M. J. Tomsic, and J. V. Marzik, Supercond. Sci. Technol. **24**, 012001 (2011).
[33]Z. X. Shi, M. A. Susner, M. Majoros, M. D. Sumption, X. Peng, M. Rindfleisch, M. J. Tomsic, and E. W. Collings, Supercond. Sci. Technol. **23**, 045018 (2010).
[34]Y. Yang, OSU dissertation (2016).
[35]Y. Yang, Hyper tech research internal report (2010).
[36]C. H. Jiang, H. Hatakeyama, and H. Kumakura, Physica C **423**, 45–50 (2005).
[37]P. Kovac, I. Husek, T. Melisek, J. C. Grivel, W. Pachia, V. Strbik, R. Diduszko, J. Homeyer, and N. H. Andersen, Supercond. Sci. Technol. **17**, L41–L46 (2004).
[38]G. Z. Li, Y. Yang, M. A. Susner, M. D. Sumption, and E. W. Collings, Supercond. Sci. Technol. **25**, 025001 (2012).
[39]M. Eisterer, M. Zehetmayer, and H. W. Weber, Phys. Rev. Lett. **90**, 247002 (2003).
[40]M. Eisterer, C. Krutzler, and H. W. Weber, J. Appl. Phys. **98**, 033906 (2005).
[41]M. Eisterer, J. Emhofer, S. Sorta, M. Zehetmayer, and H. W. Weber, Supercond. Sci. Technol. **22**, 034016 (2009).
[42]M. Eisterer, Phys. Status Sol. **2**, 1606–1614 (2005).
[43]A. Gurevich, S. Patnaik, V. Braccini, K. H. Kim, C. Mielke, X. Song, L. D. Cooley, S. D. Bu, D. M. Kim, J. H. Choi, L. J. Belenky, J. Giencke, M. K. Lee, W. Tian, X. Q. Pan, A. Siri, E. E. Hellstrom, C. B. Eom, and D. C. Larbalestier, Supercond. Sci. Technol. **17**, 278–286 (2004).
[44]A. Gurevich, Phys. Rev. B **67**, 184515 (2003).
[45]A. A. Golubov, J. Kortus, O. V. Dolgov, O. Jepsen, Y. Kong, O. K. Andersen, B. J. Gibson, K. Ahn, and R. K. Kremer, J. Phys.: Condens. Matter **14**, 1353–1360 (2002).
[46]V. Braccini, A. Gruevich, J. E. Giencke, M. C. Jewell, C. B. Eom, D. C. Larbalestier, A. Pogrebnyakov, Y. Cui, B. T. Liu, Y. F. Hu, J. M. Redwing, Q. Li, X. X. Xi, R. K. Singh, R. Gandikota, J. Kim, B. Wilkens, N. Newman, J. Rowell, B. Moeckly, V. Ferrando, C. Tarantini, D. Marre, M. Putti, C. Ferdeghini, R. Vaglio, and E. Haanappel, Phys. Rev. B **71**, 012504 (2005).
[47]K. D. Belashchenko, M. van Schilfgaarde, and V. P. Antropov, Phys. Rev. B **64**, 092503 (2001).
[48]I. I. Mazin and V. P. Antropov, Physica C **385**, 49–65 (2003).
[49]S. Oh, J. H. Kim, K. Cho, C. Lee, C.-J. Kim, S. X. Dou, M. Rindfleisch, M. Tomsic, and J.-H. Ahn, J. Appl. Phys. **106**, 063912 (2009).
[50]J. H. Kim, S. Oh, Y.-U. Heo, S. Hata, H. Kumakura, A. Matsumoto, M. Mitsuhara, S. Choi, Y. Shimada, M. Maeda, J. L. MacManus-Driscoll, and S. X. Dou, NPG Asia Mater. **4**, e3(2012).
[51]M. Bhatia, M. D. Sumption, E. W. Collings, and S. Dregia, Appl. Phys. Lett. **87**, 042505 (2005).